

Magnetic monopole field exposed by electrons

Armand B  ch  , Ruben Van Boxem, Gustaaf Van Tendeloo, and Jo Verbeeck
EMAT, University of Antwerp, Groenenborgerlaan 171, 2020 Antwerp, Belgium

The experimental search for magnetic monopole particles^{1–3} has, so far, been in vain. Nevertheless, these elusive particles of magnetic charge have fueled a rich field of theoretical study^{4–10}. Here, we created an approximation of a magnetic monopole in free space at the end of a long, nanoscopically thin magnetic needle¹¹. We experimentally demonstrate that the interaction of this approximate magnetic monopole field with a beam of electrons produces an electron vortex state, as theoretically predicted for a true magnetic monopole^{3,11–18}. This fundamental quantum mechanical scattering experiment is independent on the speed of the electrons and has consequences for all situations where electrons meet such monopole magnetic fields as for example in solids. The setup not only shows an attractive way to produce electron vortex states but also provides a unique insight into monopole fields and shows that electron vortices might well occur in unexplored solid-state physics situations.

Magnetic monopoles have provided a rich field of study, leading to a wide area of research in particle physics^{4–6}, solid state physics⁷, ultra-cold gases⁸, superconductors⁹, cosmology⁴, and gauge theory¹⁰. As electric charges can be seen as monopole sources and sinks of electric field lines, the strong symmetry with magnetic and electrical fields e.g. in the free space Maxwell equations^{19–21} hints to the possible existence of magnetic monopoles as well. So far, the search for such magnetic monopoles has been unsuccessful. However, an effective monopole field can be produced at the tip of a nanoscopic magnetized ferromagnetic needle^{11,17}. The Aharonov-Bohm effect¹² can be used to understand the effects of such a monopole field on its surroundings which is crucial to its observation and provides a better grasp of fundamental physical theory. Previous studies have been limited to theoretical semi-classical optical calculations of the motion of electrons in such a monopole field¹³. Solid state systems like the recently studied ‘spin ice’ provide a constrained system to study similar fields, but make it impossible to separate the monopole from the material⁷. Here, we realize the diffraction of fast electrons on the magnetic monopole field generated by the extremity of a long magnetic needle. Free space propagation of the electrons helps to understand the dynamics of the electron-monopole system without the complexity of a solid state system and will allow various areas of physics to use the effects of monopole fields. Various predictions about angular momentum, paths of travel and general field effects can readily be studied using the available equipment. The experiment performed here shows that even without a true magnetic monopole particle, the theoretical background on monopoles serves as a basis for experiments.

Indeed it has been predicted that when a plane electron wave interacts with a hypothetical magnetic monopole, a vortex electron state would arise^{3,11–18}:

$$\Psi_{out} = \Psi_{in} \exp(im\phi), \quad (1)$$

with m depending on the charge of the magnetic monopole and ϕ the azimuthal angle in the plane perpendicular to the electron wave propagation.

Approximating the magnetic monopole now by the end

of a magnetic needle leads to similar effects. Indeed, such a semi-infinite cylinder of magnetic flux has been considered in earlier work on magnetic monopoles but has remained a Gedanken experiment so far²². From the description of the monopole field by a vector potential, a flux line, or ‘Dirac string’ arises as a mathematical pathology which should be undetectable if a magnetic monopole was to be a true monopole, leading to the famous magnetic charge quantization¹.

The magnetic vector potential is a mathematical tool used in quantum physics which has real, measurable effects¹² which were experimentally demonstrated by electron diffraction^{18,23}. The Aharonov-Bohm (AB) phase is acquired by an electron when its path encloses magnetic flux:

$$\Delta\phi_{AB} = \frac{e}{\hbar c} \oint \mathbf{A} \cdot d\mathbf{s}. \quad (2)$$

This phase is a purely quantum mechanical effect as it is present even if the electron does not cross a region containing magnetic flux, a case where classical forces have no influence on the passing electrons. The Aharonov-Bohm effect is most often discussed with infinite cylinders of magnetic flux, avoiding the interesting end points where the magnetic field $\mathbf{B} = \text{rot}\mathbf{A}$, takes the form of a monopole:

$$\mathbf{B} = \frac{\mathbf{r}}{r^3} \quad (3)$$

If one calculates the Aharonov-Bohm phase for electrons passing perpendicular by a semi-infinite cylinder of flux, one obtains a linear azimuthal dependency around the ending point of the cylinder²⁴:

$$\Delta\phi_{AB} = \frac{2e}{\hbar c} g\phi. \quad (4)$$

This means that a passing electron will indeed be transformed into a vortex state:

$$\Psi_{out} = \Psi_{in} \exp(im\phi). \quad (5)$$

For a true monopole field, where the charge g is quantized, this leads to an integer m ($g = m\hbar c/(2e)$), resulting

in a perfect phase vortex of topological charge m . There are several different derivations of this phase factor, all extensively discussed in literature, and all predicting the same vortex phase factor^{3,22,24}. A sketch and discussion on the subtle differences between the effect of a semi-infinite cylinder of flux and a true monopole is given in Supp. Fig. 8.

Carefully tuning a magnetic needle leads to the same phase structure which is indistinguishable from a true monopole as long as the needle is thin and the flux converges towards a quantized flux. In this letter we successfully produced an approximation to a Dirac string with a nanoscopic magnetized ferromagnetic needle. The interaction of a plane electron wave with only one end of the needle allows the typical azimuthal AB phase shift to occur and vortex electron states to be created, as sketched in Fig. 1a.

From an experimental point of view, the needle is extracted from bulk Ni making use of a focused ion beam (FIB) instrument, resulting in a cone approximating an elongated cylinder with a cone angle of about 2 degrees shown in Fig. 1b. The strong shape anisotropy between the needle length (21.4 μm) and the tip diameter of only 200 nm leads to a situation where only a single on-axis magnetic domain occurs. After shaping the needle, it is positioned over a 20 μm circular aperture drilled in a nonmagnetic Au coated thin SiN film, in order to make sure electrons can only interact with one end of the needle and its magnetic monopole field.

We can verify the magnetic state at the tip of the nickel needle (red square in Fig. 2a) by inserting it in a transmission electron microscope (TEM) and performing electron holography in field free conditions^{11,18}, sketched in Supp. Fig. 1. This method measures the Aharonov-Bohm phase shift of the electrons caused by the magnetic vector potential around the needle. The resulting experimental phase map is shown in Fig. 2b and reveals the typical spiraling character in qualitative agreement with a finite element simulation for the same shape given in Fig. 2(c) and Supp. Fig. 2. The phase image resembles that of optical spiral phase plates, as used to create optical vortices²⁵. Exposing the needle to an external on-axis magnetic field flips the axis of magnetization without going through multi domain states (Supp. Fig. 3). When the magnetization direction is reversed, the handedness of the phase reverses as expected (Supp. Fig. 3). In this sense, the needle tip behaves as a magnetic monopole with a polarity that can be chosen depending on the magnetization direction.

Illuminating the needle with a plane electron wave (300 kV, $\lambda = 1.97$ pm) inside a TEM allows to experimentally verify whether a magnetic monopole field creates a vortex electron state. A series of images is recorded in the far field at different defocus of an imaging lens showing, in Fig. 3a, the presence of a central dark region. This persistent area of destructive interference is a clear sign of a phase discontinuity in the center, as expected for vortex waves. The ring is not exactly closed which occurs when a

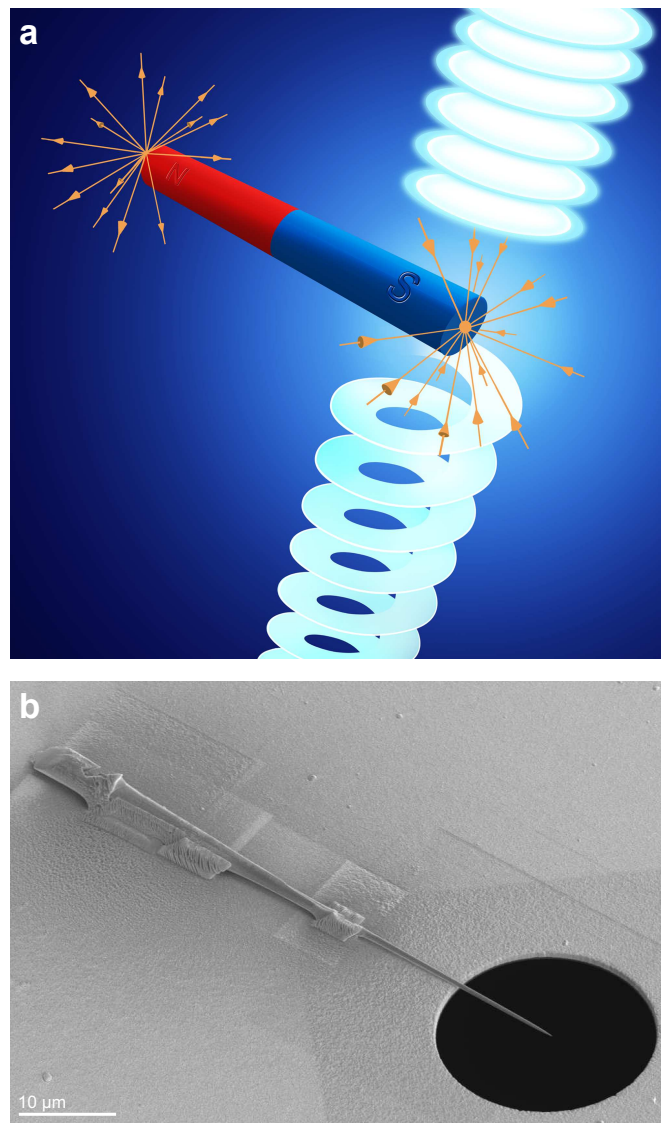


FIG. 1: *Concept and design of the monopole field: (a) An incoming electron plane wave is transformed into a vortex beam with a helical wavefront, through interaction with the magnetic monopole field. (b) SEM view of the experimental design. The nickel needle and its copper base are soldered to a gold plated SiN aperture using FIB assisted Pt deposition. Half the Ni needle is positioned over a 20 μm circular aperture, forming a local monopole field.*

non-integer orbital angular momentum is present²⁶. Decomposing the phase map over the full aperture for the simulated magnetized needle into OAM eigenmodes indeed indicates that the deviation from a pure cylindrical shape leads to a distribution of OAM eigenmodes with an average of $-5.8\hbar$ per electron (Supp. Fig. 5). These experimental observations agree remarkably well with wave optical simulations presented in Fig. 3b ruling out the possibility that the dark region is caused by a shadowing

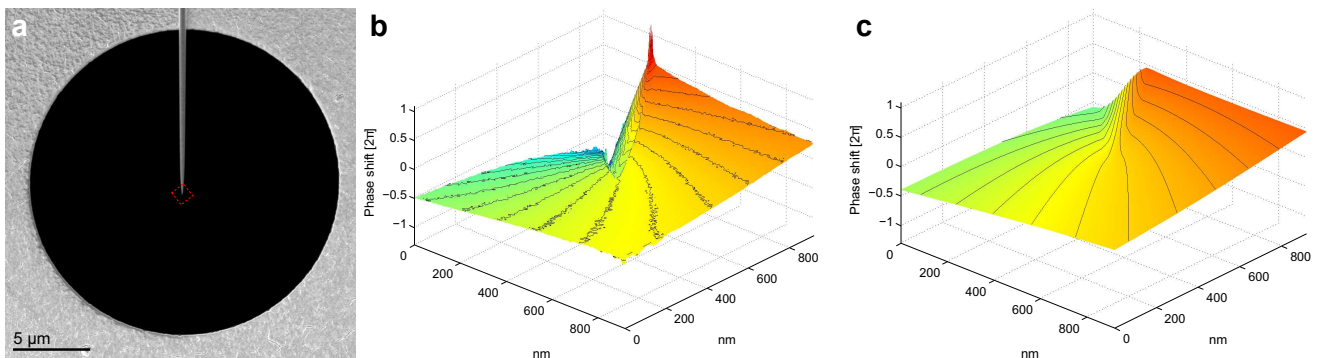


FIG. 2: *Effect of the needle on the phase of the electrons: (a) Magnified SEM image of the needle positioned onto the circular aperture. The red dashed square region indicates the position of images b and c. (b) Experimental phase map caused by the magnetic field around the Ni needle obtained by electron holography in field free conditions. The phase map is drawn in 3D to emphasize its helicity. (c) Finite element simulation of the phase map around a model for the needle. Detailed phase profiles are supplied in Supp. Fig. 4.*

effect (see Supp. Fig. 6 for further simulations).

We can also prove experimentally that this electron wave now possesses net orbital angular momentum, induced by the interaction with the monopole field, making use of the Gouy phase method^{27,28}, sketched in Supp. Fig. 1. For waves with net OAM we expect a π rotation of the image when going through focus with a direction of rotation depending on the sign of the OAM. This exact behavior is observed in Fig. 3c, which shows a clear clockwise rotation when going from under to over-focus.

These experiments show that our approximation to a Dirac string indeed provides a magnetic monopole field. The difference between a true monopole and this approximation lies in the effects of the flux returning to the needle making the field divergence free again as can be seen from the defocused images showing Fresnel fringes from the edge and a reconnection of the phase over the needle (Fig. 3a). This effect is the reason why no forked fringes are observed in the experimental holograms (Supp. Fig. 3a,b). Detailed holographic simulations showing this subtle reconnection difference between a true monopole and a Dirac string are shown in Supp. Fig. 7 together with a sketch explaining the creation of the phase singularities in both cases (Supp. Fig. 8).

The further we go into the far field, the more this effect of the needle disappears and the more the resulting wave becomes a true electron vortex as if the interaction took place with a real monopole. It is expected that a needle presenting an integer charge will allow a vortex with sufficient purity to heal itself, removing this distortion²⁹.

The above experiment shows how quantum experiments with magnetic monopoles are feasible and provides a very promising way to make electron vortices for applications in electron microscopy with an almost eight fold gain in beam intensity while avoiding other unwanted beams as compared to currently used holographic reconstruction methods^{13,30}. The current device is static and its magnetic polarization depends entirely on the shape

and material of the needle. However, there are no fundamental obstacles to create a nanoscale solenoid in order to provide any flux in the Dirac string depending on applied current. This extension would provide a dynamically switchable source of vortex electrons which would be highly desirable to improve the speed, flexibility and signal to noise ratio in vortex electron experiments.

Even though an electron microscope was used to conveniently demonstrate the effect, the consequences of this experiment reach much further as the AB effect is independent on the speed of the electrons and vortex states can be generated in e.g. solid state systems where conduction electrons encounter similar monopole fields. Indeed if a sufficiently coherent electron wave packet in a material would encounter a similar approximate monopole field (e.g. generated by a ferromagnetic inclusion), it would gain a topologically protected azimuthal phase, possibly changing its propagation dynamics.

I. METHODS

The needle was prepared from bulk nickel by a focused ion beam instrument (FIB) using a FEI Helios Nanolab with Ga ions accelerated to 30 kV. After extraction from the bulk sample, a large nickel chunk ($\sim 10 \times 3 \times 30 \mu\text{m}^3$) was welded onto an already prepared conical shaped copper base and thinned concentrically. The resulting needle is $21.4 \mu\text{m}$ long, 700 nm wide at the bottom and 200 nm at the top. The nickel needle and part of its copper base were then extracted and sealed over a gold plated SiN film. The needle was precisely placed in order for half of its length to hang over a $20 \mu\text{m}$ circular aperture previously drilled in the Au/SiN film. Electron holography was performed in Lorentz (field free) mode at 300 kV on the QuAntEM microscope (a double corrected Titan³ 80-300) and is sketched in Supp. Fig. 1. The Möllensted

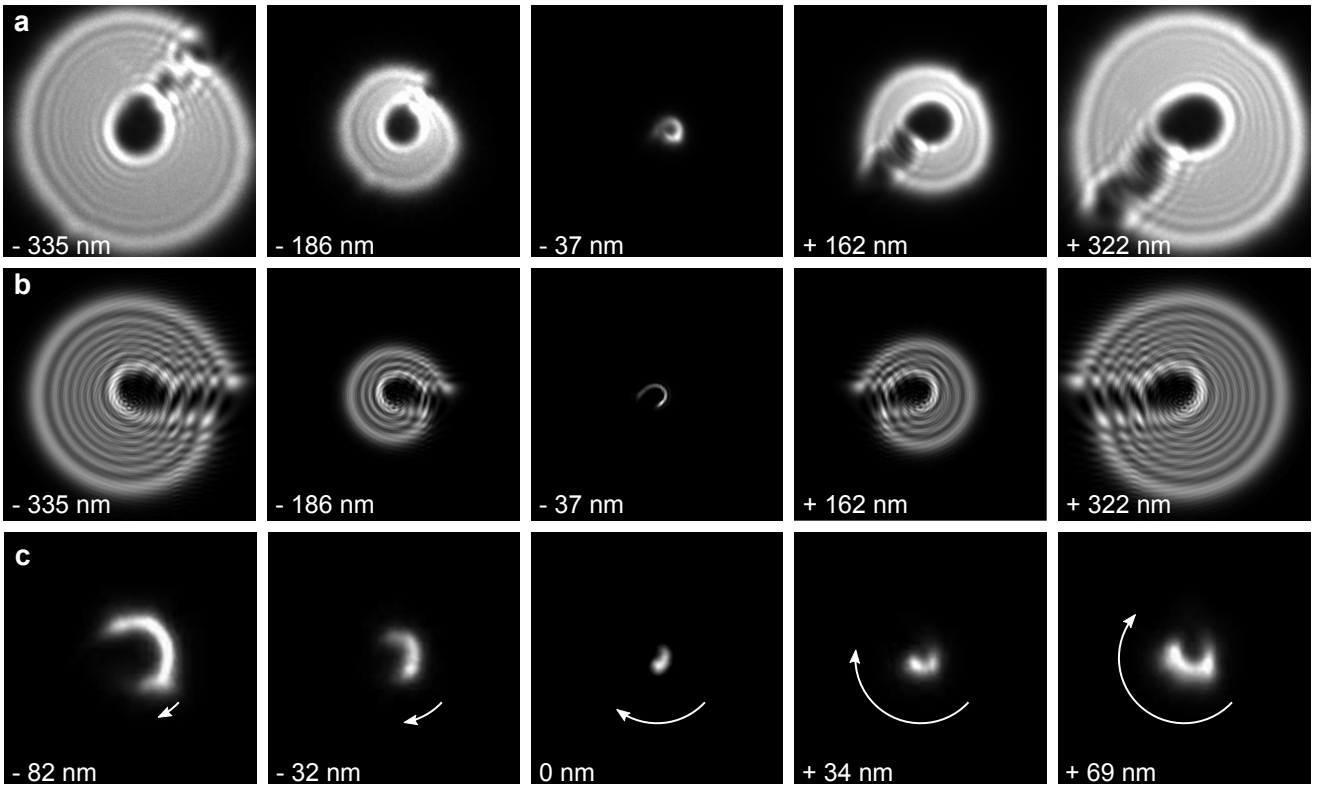


FIG. 3: Electron vortex states observed after interaction with the monopole field: (a) Through focus series of the needle aperture in the diffraction plane. Note the persistent dark region in the centre caused by destructive interference typical for vortex waves. The near-focus central image shows a doughnut like intensity profile, typical of a vortex beam which opens on one side and indicating a non-integer total orbital angular momentum. (b) Wave optical simulation obtained by Fourier transforming the complex wave from Fig.2c with a Fresnel defocus applied. Note the detailed agreement with the experimental figures in (a). A similar simulation assuming no azimuthal phase is given in Supp. info showing a very different behavior ruling out the possibility that the black region is caused by shadowing effects from the needle. Intensity profiles are also given in Supp. info. (c) Through focus series of the beam half cut by a sharp edge. The rotation of the image along the series proves the presence of a net negative orbital angular momentum.

biprism voltage was set to +180 V in order to have a large field of view and good sampling of the interference fringes. The phase maps were reconstructed from holograms using the standard Fourier filtering method with a final unwrap step. Such phase maps suffer from the presence of the electrostatic potential which is corrected by flipping the magnetisation of the needle and subtracting the phase maps obtained from two opposite magnetisations. The magnetisation state of the needle is changed by tilting the needle 30 degrees and applying

a small magnetic field (~ 0.15 T) by raising the current in the objective lens to 5% of its full strength. Through focus series were recorded in the diffraction plane of the Lorentz lens using the highest camera length available (18 m) and recorded on a CCD mounted at the end of a Gatan Quantum Image Filter. The Gouy phase experiment was realized in the exact same conditions, cutting the beam with the sharp edge of an objective aperture to clearly see the rotation effects (Supp. Fig. 1).

¹ Dirac, P. A. M. Quantised singularities in the electromagnetic field. *Proceedings of the Royal Society of London. Series A* **133**, 60–72 (1931).

² Milton, K. A., Kalbfleisch, G. R., Luo, W. & Gamberg, L. Theoretical and experimental status of magnetic monopoles. *International Journal of Modern Physics A*

17, 732–747 (2002).

³ Wu, T. T. & Yang, C. N. Dirac monopole without strings: Monopole harmonics. *Nuclear Physics B* **107**, 365 – 380 (1976).

⁴ Bonnardeau, M. & Drukier, A. K. Creation of magnetic monopoles in pulsars. *Nature letters* **277**, 543–544 (1979).

- ⁵ Frisch, H. J. Quest for magnetic monopoles. *Nature* **344**, 706–707 (1990).
- ⁶ Aad, G. *et al.* Search for magnetic monopoles in $\sqrt{s} = 7$ TeV pp collisions with the atlas detector. *Phys. Rev. Lett.* **109**, 261803 (2012).
- ⁷ Castelnovo, C., Moessner, R. & Sondhi, S. L. Magnetic monopoles in spin ice. *Nature* **451**, 42–45 (2008).
- ⁸ Salomaa, M. M. Monopoles in the rotating superfluid helium-3 ab interface. *Nature* **326**, 367–370 (1987).
- ⁹ Cardoso, M., Bicudo, P. & Sacramento, P. D. Confinement of monopole field lines in a superconductor at $t \neq 0$. *Annals of Physics* **323**, 337 – 355 (2008).
- ¹⁰ Goddard, P. & Olive, D. I. Magnetic monopoles in gauge field theories. *Reports on Progress in Physics* **41**, 1357 (1978).
- ¹¹ Kasama, T., Antypas, Y., Chong, R. K. & Dunin-Borkowski, R. E. Novel approaches for the characterization of electromagnetic fields using electron holography. *MRS Proceedings* **839** (2004).
- ¹² Aharonov, Y. & Bohm, D. Significance of electromagnetic potentials in the quantum theory. *Phys. Rev.* **115**, 485–491 (1959).
- ¹³ Kruit, P. & Lenc, M. Optical properties of the magnetic monopole field applied to electron microscopy and spectroscopy. *Journal of Applied Physics* **72**, 4505–4513 (1992).
- ¹⁴ Bliokh, K. Y., Bliokh, Y. P., Savel'ev, S. & Nori, F. Semiclassical dynamics of electron wave packet states with phase vortices. *Phys. Rev. Lett.* **99**, 190404 (2007).
- ¹⁵ Uchida, M. & Tonomura, A. Generation of electron beams carrying orbital angular momentum. *Nature* **464**, 737–739 (2010).
- ¹⁶ Verbeeck, J., Tian, H. & Schattschneider, P. Production and application of electron vortex beams. *Nature* **467**, 301–304 (2010).
- ¹⁷ Fukuhara, A., Shinagawa, K., Tonomura, A. & Fujiwara, H. Electron holography and magnetic specimens. *Phys. Rev. B* **27**, 1839–1843 (1983).
- ¹⁸ Tonomura, A. *et al.* Observation of aharonov-bohm effect by electron holography. *Phys. Rev. Lett.* **48**, 1443–1446 (1982).
- ¹⁹ Berry, M. V. Optical currents. *Journal of Optics A: Pure and Applied Optics* **11**, 094001 (2009).
- ²⁰ Bliokh, K. Y., Bekshaev, A. Y. & Nori, F. Dual electromagnetism: helicity, spin, momentum and angular momentum. *New Journal of Physics* **15**, 033026 (2013).
- ²¹ Cameron, R. P. & Barnett, S. M. Electricmagnetic symmetry and noether's theorem. *New Journal of Physics* **14**, 123019 (2012).
- ²² Lipkin, H. J. & Peshkin, M. Angular momentum paradoxes with solenoids and monopoles. *Physics Letters B* **118**, 385 – 390 (1982).
- ²³ Chambers, R. G. Shift of an electron interference pattern by enclosed magnetic flux. *Phys. Rev. Lett.* **5**, 3–5 (1960).
- ²⁴ Wilczek, F. Magnetic flux, angular momentum, and statistics. *Phys. Rev. Lett.* **48**, 1144–1146 (1982).
- ²⁵ Beijersbergen, M., Coerwinkel, R., Kristensen, M. & Woerdman, J. Helical-wavefront laser beams produced with a spiral phaseplate. *Optics Communications* **112**, 321 – 327 (1994).
- ²⁶ Berry, M. V. Optical vortices evolving from helicoidal integer and fractional phase steps. *Journal of Optics A: Pure and Applied Optics* **6**, 259–268 (2004).
- ²⁷ Bliokh, K. Y., Schattschneider, P., Verbeeck, J. & Nori, F. Electron vortex beams in a magnetic field: A new twist on landau levels and aharonov-bohm states. *Phys. Rev. X* **2**, 041011 (2012).
- ²⁸ Guzzinati, G., Schattschneider, P., Bliokh, K. Y., Nori, F. & Verbeeck, J. Observation of the larmor and gouy rotations with electron vortex beams. *Phys. Rev. Lett.* **110**, 093601 (2013).
- ²⁹ Bouchal, Z., Wagner, J. & Chlup, M. Self-reconstruction of a distorted nondiffracting beam. *Optics Communications* **151**, 207 – 211 (1998).
- ³⁰ Verbeeck, J. *et al.* Atomic scale electron vortices for nanoresearch. *Applied Physics Letters* **99**, 203109 (2011).

II. CONTRIBUTIONS

A.B. and J.V. conceived the experiment; A.B. designed the sample and carried out the TEM measurements. All authors contributed to theory, data analysis and writing the paper.

III. CORRESPONDING AUTHOR

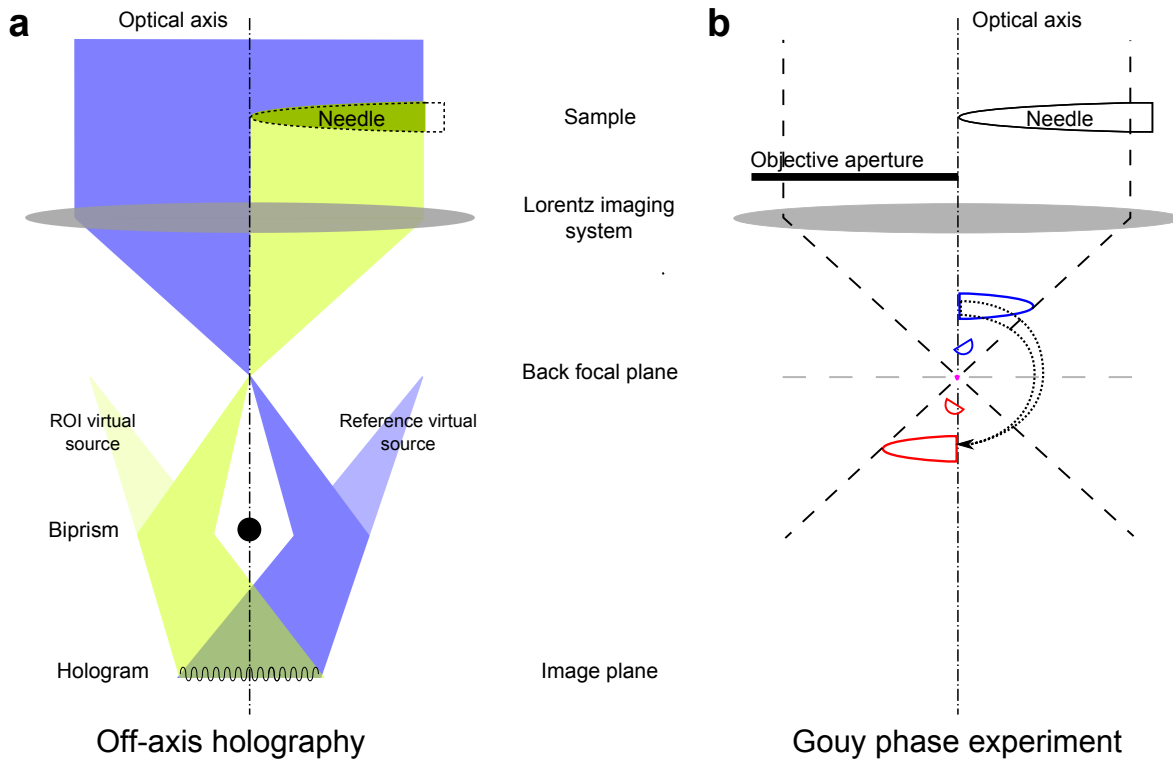
Correspondence should be addressed to J.V.: jo.verbeeck@uantwerp.be.

IV. ACKNOWLEDGMENTS

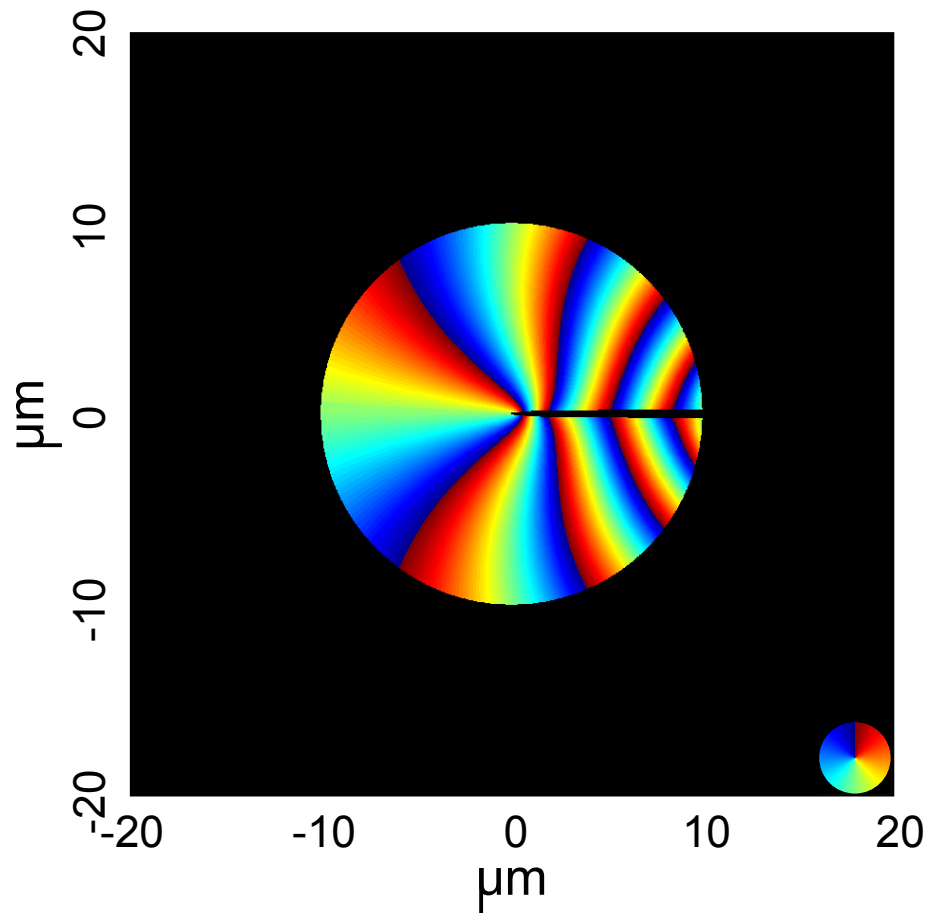
This work was supported by funding from the European Research Council under the 7th Framework Program (FP7), ERC grant 246791 COUNTATOMS and ERC Starting Grant 278510 VORTEX. The Qu-Ant-EM microscope was partly funded by the Hercules fund from the Flemish Government. The authors acknowledge financial support from the European Union under the Seventh Framework Program under a contract for an Integrated Infrastructure Initiative. Reference No. 312483-ESTEEM2. R.V.B. acknowledges a PhD fellowship grant from the FWO (Aspirant Fonds Wetenschappelijk Onderzoek Vlaanderen).

Supplementary information: Magnetic monopole field exposed by electrons

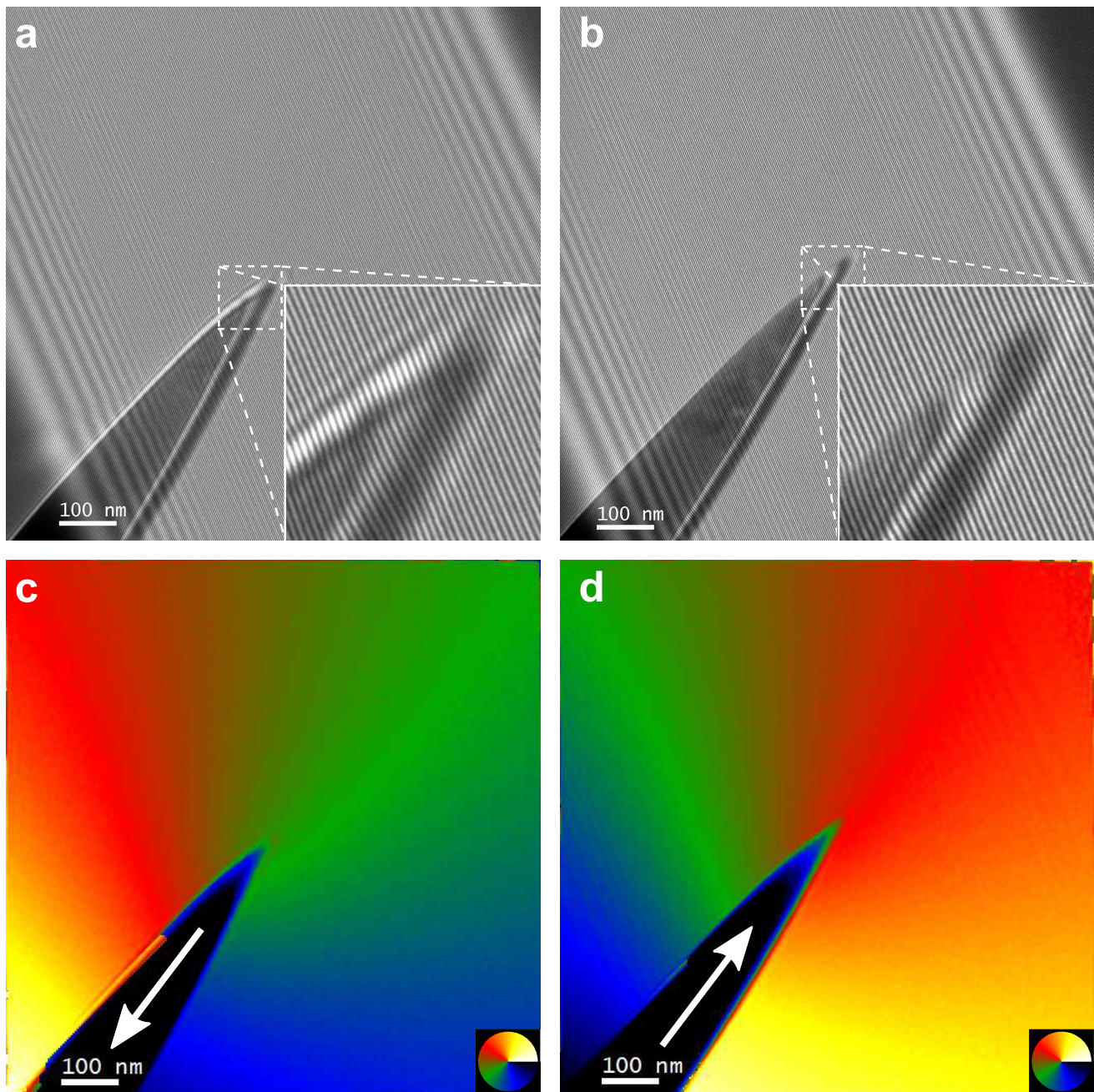
A. Béch , R. Van Boxem, G. Van Tendeloo, J. Verbeeck
EMAT, University of Antwerp, Groenenborgerlaan 171, 2020 Antwerp, Belgium



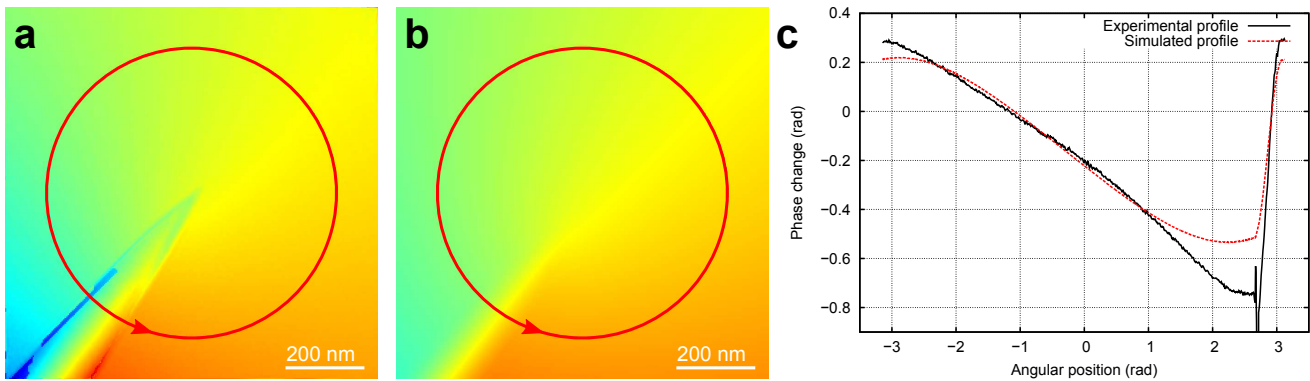
Supplementary Figure 1: *Sketches of experimental setups. (a) Off-axis holography consists of superimposing a reference wave with a wave passing through the sample. The resulting fringe pattern, the hologram, carries information about the phase of the wave. (b) The Gouy phase experiment consists of acquiring a through focus series in the back focal plane. When passing through the focus point, the shadow image flips. The insertion of a sharp edge blocking part of the beam, here an objective aperture, allows better visualisation of this image inversion. In the case of an object illuminated with a vortex beam, as sketched here, the image is not simply flipped but also rotates when going through focus in a direction given by the sign of the orbital angular momentum.*



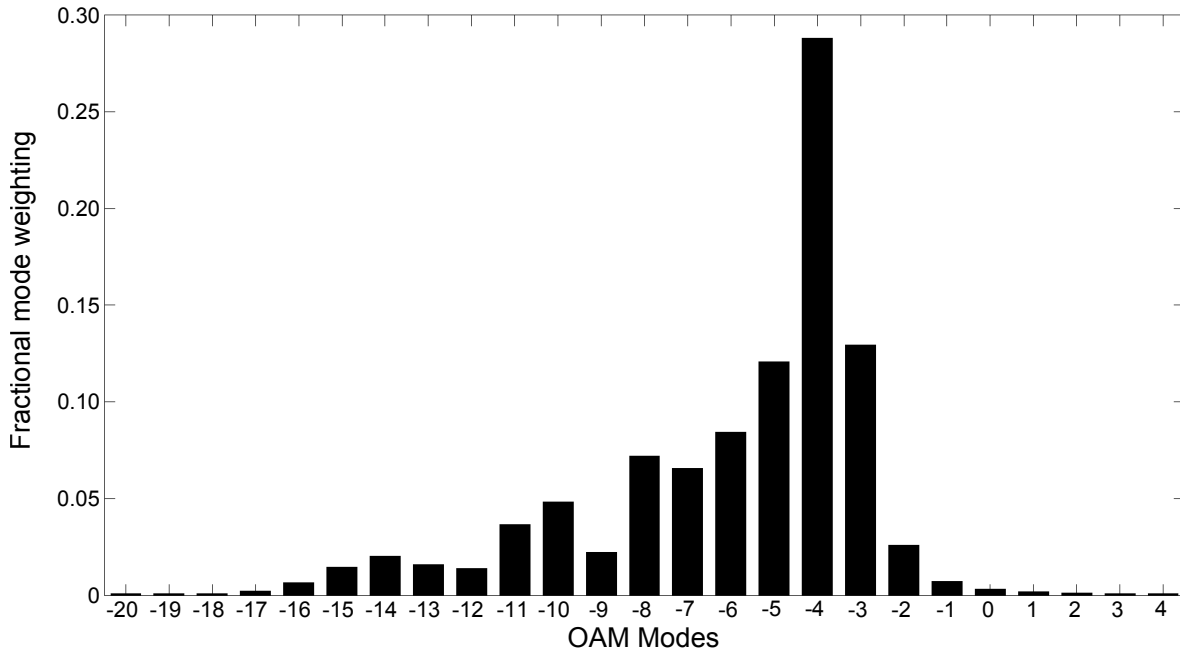
Supplementary Figure 2: *Evolution of the phase around the nickel magnetic needle over the full aperture. This phase map was calculated from finite element simulations taking into account the experimental dimensions of the needle (the scale figures a phase change of 2π). The volume magnetization value was adapted in the simulation to match the experimental change in phase around the tip (Fig.2 b). This results in a volume magnetization of $1.72e5 \text{ A.m}^{-1}$ instead of $4.88e5 \text{ A.m}^{-1}$ expected for bulk Ni. This discrepancy can be attributed to gallium implantation during the FIB preparation of the needle, reducing the effective volume of Ni which contributes to the magnetism.*



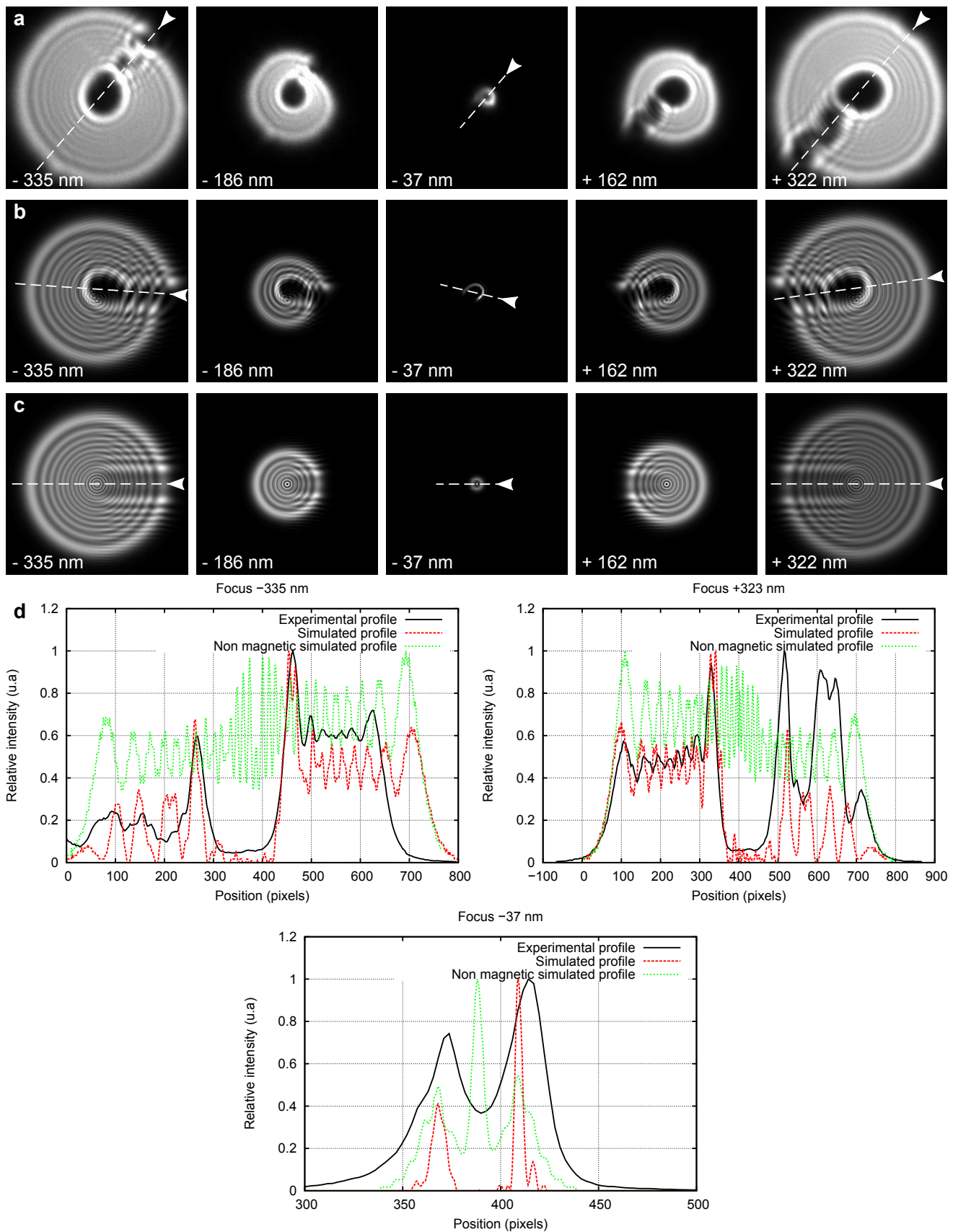
Supplementary Figure 3: *Experimental holograms and phase maps around the needle tip. (a) Experimental hologram acquired at the tip of the needle in field free conditions (Lorentz mode), the inset shows an enlarged view of the holographic fringes near the tip of the needle. Note the absence of forking fringes as further explained in Supplementary Figure 7. (b) Hologram of the same region taken after changing the direction of the magnetic field together with a magnified view of the tip as inset, also revealing the absence of forking pattern in the holographic fringes. To change the direction of the magnetic field, the needle was tilted 30° out of plane and an out of plane magnetic field of 0.15 T was applied by slightly increasing the strength of the objective lens. The lens was turned off and the needle was tilted back in plane before acquisition of the new hologram. (c) Phase map obtained from experimental holograms (a) with the magnetic field pointing into the tip of the needle. The scale figures a phase change from 0 to 4π . (d) Same image taken with the magnetic field pointing out of the needle. The reversal of the magnetization changes the handedness of the phase distribution as expected. Across the needle, a black color is used as the phase scale saturates due to the interaction with the mean inner potential of the material. The color scale is chosen this way to emphasize the magnetically induced phase. The sum of both figures (c) and (d) was used to remove the influence of the electrostatic potential and to create Fig 2.b.*



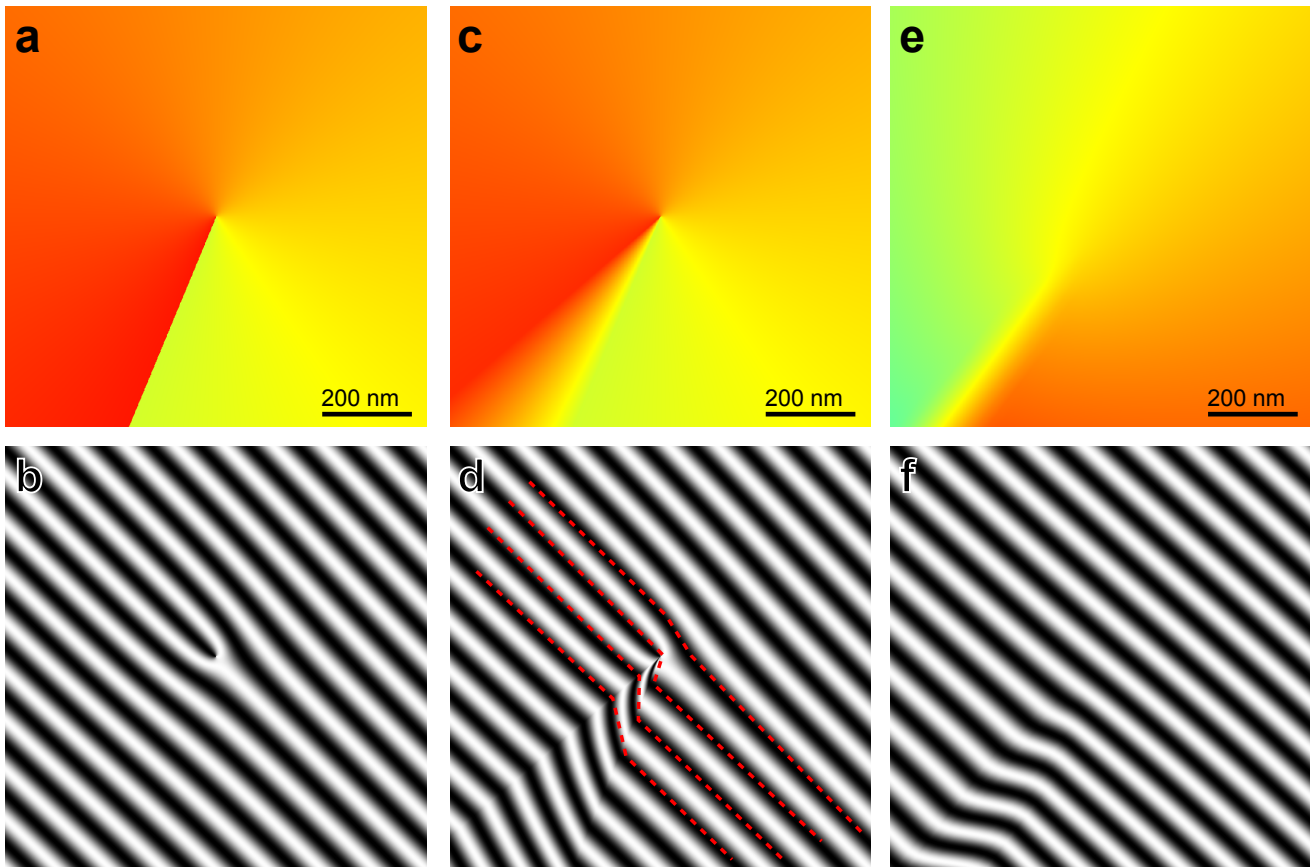
Supplementary Figure 4: Comparison of experimental and simulated phase shifts. (a) Experimental phase maps around the tip of the needle. (b) Simulated phase maps corresponding at the same position as (a). (c) Phase profiles along a circular path around both experimental (a) and simulated (b) phase maps. The radius of the integrating loop is 195 nm and the profiles starts from the arrow sketched in (a) and (b). Note the near linear phase decrease in both experimental and simulated profiles as well as the reconnection of the phase over the needle which is needed for a divergence free field. This reconnection has a subtle effect on the holograms but the majority of the electron wave 'sees' an azimuthal phase leading to a clear vortex state even though the phase is not discontinuous.



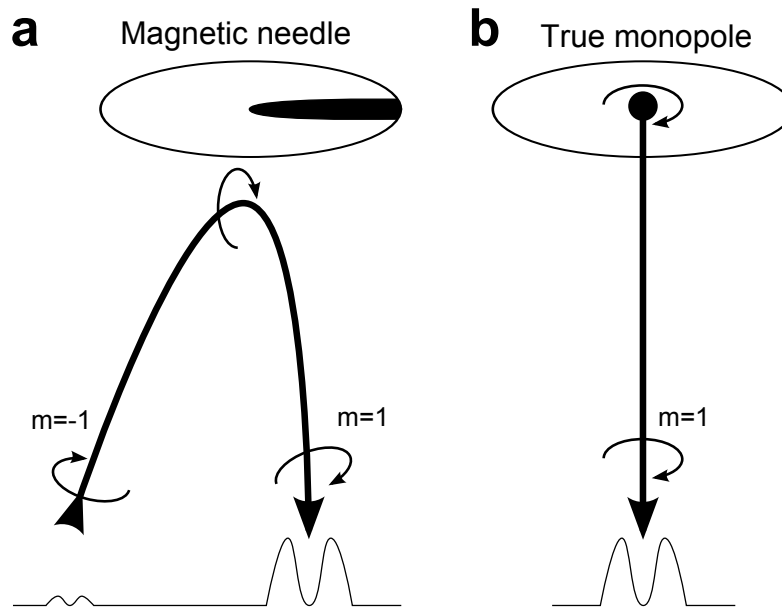
Supplementary Figure 5: OAM Eigenmodes decomposition of the simulated phase in the full aperture. The simulated phase presented in Supp. Fig. 2 was used as a source for the decomposition. Note the clear shift towards negative OAM, indicating the action of the monopole field. The width of the distribution is caused by the fact that the needle is conical as opposed to an ideal cylindrical needle which would lead to a single OAM mode.



Supplementary Figure 6: *Experimental and simulated through focus series. (a) Experimental through focus series of the electron intensity near the diffraction plane. (b) Wave optical simulations assuming the theoretical phase profile from Fig. 2c. The simulation is simply a Fourier transform of the complex wave in the needle plane with a Fresnel defocus term to simulate the effect of defocus. Note the strong similarity with the experiment. In order to rule out that the black central part in (a) is caused by a shadowing effect, an alternative simulation assuming a flat phase (no magnetic effects) profile with a totally blocking needle is given in (c). Indeed a shadow of the needle is faintly visible but contrary to the experiment the shadow is not truly black and disappears completely when in focus. These simulations provide strong evidence that a true vortex state is produced. (d) Intensity profiles are given to further*



Supplementary Figure 7: *Simulation of the effect of a phase discontinuity on the holographic fringes. (a) Phase map assuming a perfect azimuthal phase profile with $m=1$. (b) This phase profile leads to a typical forked holographic pattern. (c) Phase map presenting a continuous approximation to phase displayed in (a) with a steep but finite reconnection near the bottom left corner. (d) Resulting hologram which still resembles (b) but upon detailed inspection the fork has disappeared and all fringes are single continuous lines as emphasized by the dotted lines. (e) Theoretical phase shown also in Fig. 2c. (f) Resulting hologram. Note the similarities to (d) without bifurcations of the fringe lines in agreement with the experimental holograms (Supp. Fig. 3 a,b insets). These simulations only take into account the magnetic field effect while the electrostatic potential inside the needle is not simulated for clarity.*



Supplementary Figure 8: *Sketch of the fundamental difference between the interaction with an approximate monopole field and a true hypothetical magnetic monopole. (a) The approximate monopole field will imprint a continuously varying phase on the incoming electron wave with an azimuthal phase profile that is reconnected over the width of the needle. In the immediate vicinity of the needle there are therefore no phase singularities and no forked holographic fringes would occur if the phase is measured in this plane (this is a consequence of the field being divergence free). Nevertheless, propagating the electron wave behind the needle (going from top to bottom), the wave will develop a vortex-antivortex pair indicated by the black bent arrow. This means that two singularities arise with opposite winding number. The positive singularity remains on the optical axis and is surrounded by the majority of electron density in the wave, while the opposite singularity will split off and shift to high angles (depending on the steepness of the phase reconnection on the needle) and to a region where the electron density is nearly zero. The fact that the majority of the electron density is occurring around the main singularity also means that a real vortex state with an OAM of \hbar is created. The unwanted opposite singularity can be excluded by making use of an aperture if needed. (b) In case of a true monopole field, the situation is different and a single phase singularity is created starting from the monopole. This leads to the formation of an electron vortex wave with OAM of \hbar . Both setups therefore have nearly the same effect on the electron with the exception of the total winding number in the observation plane which is zero for an approximate monopole field and equals one for the true monopole field. Putting an aperture to cut out the region of the opposite singularity brings both cases even closer together. For all practical matters, a monopole field therefore behaves nearly identical to the field produced by a true monopole as long as we don't observe the near field area of the scattering.*